

Dielectric relaxation and study of electrical conduction mechanism in $\text{BaZr}_{0.1}\text{Ti}_{0.9}\text{O}_3$ ceramics by correlated barrier hopping model

TANUSREE MONDAL¹, SAYANTANI DAS², T.P. SINHA³, P.M. SARUN^{1,*}

¹Functional Ceramics Laboratory, Department of Applied Physics, Indian Institute of Technology (Indian School of Mines), Dhanbad-826004, India

²Department of Physics, University of Calcutta, 92, Acharya Prafulla Chandra Road, Kolkata-700009, India

³Department of Physics, Bose Institute, 93/1, Acharya Prafulla Chandra Road, Kolkata-700009, India

This work aims to study the electrical conduction mechanism in the dielectric material $\text{BaZr}_{0.1}\text{Ti}_{0.9}\text{O}_3$ (BZT) ceramics by applying AC signal in the frequency range of 10^2 Hz to 10^6 Hz. The phase purity and microstructure of the sample have been studied by X-ray diffraction refinement and field-emission scanning electron microscope (FE-SEM) analysis. The appearance of resonance peaks in the loss tangent at high temperature is due to inherent dielectric relaxation processes of this oxide. The temperature dependent Cole-Cole plot has been studied in details to determine both the grain and grain boundary contribution to the conductivity. Electrical modulus analysis reveals that the hopping of charge carriers is the most probable conduction mechanism in BZT ceramics. The obtained data of AC conductivity obey the universal double power law and have been discussed in terms of microstructural network characteristics. The behavior of frequency exponent n of AC conductivity as a function of temperature verify the applicability of the correlated barrier hopping (CBH) model. The AC conductivity data are used to estimate the minimum hopping length, density of states at Fermi level, thermal conductivity and apparent activation energy. The value of activation energy confirms that the oxygen vacancies play a vital role in the conduction mechanism.

Keywords: *Rietveld refinement; dielectric relaxation; electrical conductivity mechanism; correlated barrier hopping model*

1. Introduction

Since the past few decades, enormous interest has been observed to develop lead-free perovskites for their excellent electrical properties and environment-friendly nature. $\text{BaZr}_x\text{Ti}_{1-x}\text{O}_3$ (BZT) is one of lead free ferroelectric materials most frequently used in various technological applications, namely, in the electronic industry as multilayer ceramic capacitors (MLC), piezoelectric actuators, sensors, micro-electromechanical systems (MEMS) and in manufacture of electro-optical devices [1–4]. However, BaTiO_3 – BaZrO_3 solid solution is of great interest among researchers due to the change in dielectric response that can lead to normal ferroelectric behavior as well as diffuse phase transition to relaxor behavior with

variation of Zr concentration [5–7]. $\text{BaZr}_{0.1}\text{Ti}_{0.9}\text{O}_3$ composition is chosen as the basic solid solution because it lies in the boundary between the normal and diffuse phase transition region and among $\text{BaZr}_x\text{Ti}_{1-x}\text{O}_3$ compositions, it shows high dielectric and piezoelectric properties [8–10].

The dielectric relaxation and the conduction mechanism of $\text{BaZr}_{0.1}\text{Ti}_{0.9}\text{O}_3$ at higher temperature has been less studied. A comparative study of impedance behavior of BZT with the variation of Zr concentration has been presented [11]. However, this is not enough to understand the whole mechanism of dielectric relaxation and conduction mechanism of $\text{BaZr}_{0.1}\text{Ti}_{0.9}\text{O}_3$ ceramics. In titanate based perovskite materials, ionized oxygen vacancies are considered as mobile charge carriers [12–14]. At high temperature, the oxygen vacancies can be thermally ionized very easily by releasing the free electrons which eventually become conduction

*E-mail: sarun.res@gmail.com

electrons. The presence of these conduction electrons significantly affects the dielectric relaxation of BZT, hence, it is essential to gain a fundamental understanding of their conduction mechanism at high temperature. Moreover, the electrical properties of dielectric materials are significantly affected by intrinsic properties as well as extrinsic properties such as grain, grain boundary phenomena, and electrode sample interface. Alternating current (AC) conductivity is extensively used to study the electrical processes that occur in the polycrystalline ceramic materials and it is commonly used to correlate the electrical response characteristics of the material to the microstructural network. For better understanding of charge transport in the material, AC conductivity has been discussed in terms of various theoretical models.

Hence, in the present work, a systematic study of temperature and frequency dependent dielectric relaxation and electrical conductivity of $\text{BaZr}_{0.1}\text{Ti}_{0.9}\text{O}_3$ ceramics are investigated by means of complex impedance and electrical modulus spectroscopy. The concept of correlated barrier hopping (CBH) model has been incorporated to the AC conductivity analysis to understand the charge transport mechanism in $\text{BaZr}_{0.1}\text{Ti}_{0.9}\text{O}_3$ ceramics. Furthermore, the density of states at Fermi level, the minimum hopping length and thermal conductivity are also estimated using AC conductivity analysis.

2. Experimental

$\text{BaZr}_{0.1}\text{Ti}_{0.9}\text{O}_3$ ceramics was prepared by solid state reaction method, using high purity BaCO_3 , TiO_2 and ZrO_2 oxide powders (Alfa Aesar > 99.9 %) as starting ingredients. Stoichiometrically weighed ingredients were thoroughly mixed and ground in acetone medium using an agate mortar and subsequently calcined in air at 1300 °C for 4 h. The calcined powder was homogenized in acetone medium and subsequently dried. PVA (polyvinyl alcohol) of 3 wt.% was used as a binder with the calcined powder during the preparation of pellets, having thickness of ~1.4 mm and diameter of ~12 mm under a pressure of 175 MPa.

These pellets were sintered at 1350 °C for 4 h in a muffle furnace (Electroheat, Naskar Co., Kolkata), equipped with a digital temperature controller (Eurotherm 2404) with an accuracy of ± 1 °C.

The sintered BZT sample was analyzed by a powder X-ray diffractometer (Rigaku Miniflex II) using $\text{CuK}\alpha$ radiation. Microstructural analysis of the sample was done using a field emission scanning electron microscope (FE-SEM; ZEISS Supra-55). To perform dielectric characterization, the conducting silver paste was coated on both sides of the pellet and cured at 150 °C for 2 h. Dielectric and impedance parameters of BZT were measured as a function of temperature in the wide frequency range (40 Hz to 1 MHz) using LCR meter (Hioki-3552, Japan).

3. Results and discussion

The X-ray diffraction pattern of the sintered BZT sample is shown in Fig. 1a. All the peaks are indexed according to the standard X-ray pattern of the tetragonal BaTiO_3 (ICDD PDF-2 Card No. 05-0626). The figure shows that the sample contains only the peaks corresponding to BZT. No other secondary phase is observed. The result confirms the formation of pure perovskite BZT phase. The peak splitting (0 0 2) and (2 0 0) at $2\theta \sim 45^\circ$ of the XRD pattern indicates its tetragonal symmetry. Rietveld refinement has been carried out on the XRD pattern to confirm this. The structural refinement was done by the Fullprof program [15]. According to the literature [16], the equality of structural refinement is generally controlled by R-values (R_{wp} , R_{p} , R_{exp} , R_{Bragg} and χ^2). After the refinement, the values obtained for R's and χ^2 have been listed in Table 1. They all belong to the tetragonal phase structure with a space group $P4\text{mm}$. The difference in the plots between observed and calculated patterns confirms the success of the Rietveld refinement (Fig. 1b).

Fig. 2 shows a FE-SEM image of the fractured surface of BZT sample. The domain structure of BZT ceramics with “lamellar” and water-mark characters is clearly observed in the FE-SEM image as indicated by the circles in Fig. 2.

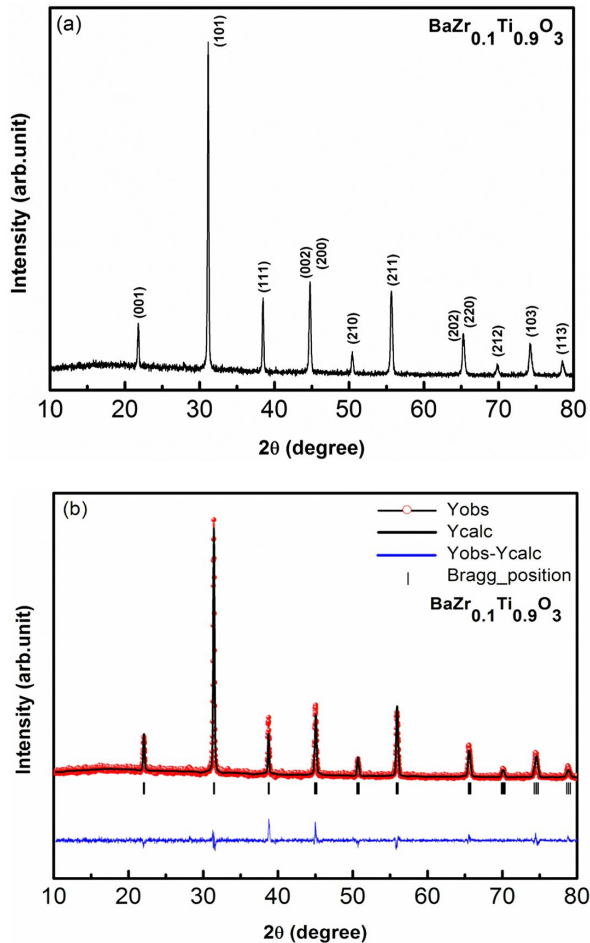


Fig. 1. (a) X-ray diffraction pattern of $\text{BaZr}_{0.1}\text{Ti}_{0.9}\text{O}_3$ ceramics. (b) Rietveld refinement of XRD pattern of BZT ceramics.

The figure shows a clean microstructure with well-defined grain boundaries. The size distribution of the formed grains is found to be nonuniform. The clean grain boundary is the result of low surface energy at the contact interface of two grains due to elastic deformation, which promotes efficient interdiffusion of ions during the sintering process. The intradiffusion process within the grain leads to the formation of lamellar structure of the grains.

Fig. 3a shows the angular frequency ($\omega = 2\pi f$) dependency of the real part of complex dielectric permittivity ϵ' in the paraelectric temperature region from 553 K to 673 K. ϵ' decreases with increasing frequency in the entire temperature range. The application of electric field

Table 1. Lattice parameters, unit cell volume, c/a ratio and atomic positions for the $\text{Ba}(\text{Zr}_{0.1}\text{Ti}_{0.9})\text{O}_3$.

Atoms	Wyckoff	Site	x	y	z
Ba	1a	4mm	0	0	0
Ti	1b	4mm	0.5	0.5	0.51305
Zr	1b	4mm	0.5	0.5	0.51305
O1	1b	4mm	0.5	0.5	0.01615
O2	2c	2mm	0.5	0	0.48612

$P4mm$ (99) – tetragonal ($a = b = 4.021 \text{ \AA}$; $c = 4.036 \text{ \AA}$; $c/a = 1.004$; $V = 65.26 \text{ \AA}^3$) $R_{\text{Bragg}} = 7.14$; $R_p = 44.1$; $R_{\text{wp}} = 30.9$; $R_{\text{exp}} = 26.18$; $\chi^2 = 1.40$.

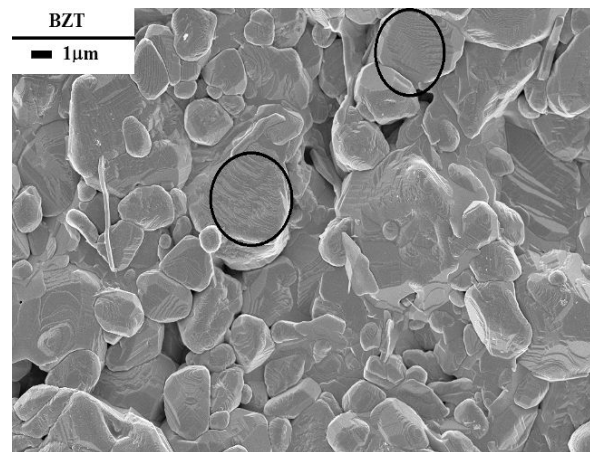


Fig. 2. FE-SEM micrograph of BZT ceramics. The domain structure with lamellar and water-mark characters is marked with the circles in the FE-SEM image.

induces static dipoles in the material. Since the electric field changes its polarity with time, the induced dipoles also follow the alternating field at lower frequencies ($\omega \ll 1/\tau$ with $\epsilon' \approx \epsilon_s$, where τ is the relaxation time and ϵ_s is the value of dielectric constant at quasi-static field). As the frequency increases, dielectric permittivity slightly decreases because dipoles begin to lag behind the field. Dielectric permittivity drops (relaxation process) sharply when the frequency reaches the characteristic frequency ($\omega = 1/\tau$). At the higher frequency region ($\omega \gg 1/\tau$) dipoles do no longer follow the field and the value of dielectric permittivity becomes almost frequency independent (hence $\epsilon' \approx \epsilon_\infty$, where ϵ_∞ is the value of ϵ' at high frequency). Moreover, at high temperature,

polarization occurs because of free movement of charge carriers through the crystal. The higher values of dielectric constant (ϵ') at low frequencies are due to the accumulation of free charges at the grain boundary, whereas, the observed low ϵ' at high frequency is attributed to the lower dielectric constant of the grains [17–19]. The variation of dielectric loss ($\tan\delta$) with frequency for different temperatures is shown in Fig. 3b. The figure shows the existence of $\tan\delta$ peaks which correspond to the relaxation process that shifts to higher frequency region with increasing temperature. This observed phenomenon suggests that charge carrier concentration increases in the material due to thermal agitation at elevated temperature. The peaks observed for $\tan\delta$ are attributed to the fact that the hopping frequency of the charge carriers is approximately equal to the frequency of the external applied field [20].

Complex plane impedance plot gives the information about the electrical properties of a sample. The impedance properties usually occur due to the intragrain, intergrain and electrode processes. There are many ways by which the motion of charges can occur, namely, dipole re-orientation, space charge formalism and charge displacement. Polycrystalline material contains both grain and grain boundaries which lead to two semicircular arcs in the Nyquist diagram. Each semicircular arc can be interpreted as a parallel resistance-capacitance (RC) circuit in the ideal case or the same can be modeled as resistance-constant phase element (R-CPE) network. Fig. 4a shows Nyquist plot (Z'' vs. Z') of BZT sample over a wide range of frequency for different temperatures. The figure shows two successive semicircular arcs and each arc is best fitted with two parallel combinations of resistor-CPE (RQ) elements as shown in the figure. The presence of two semicircle arcs implies that the polarization mechanism in the BZT ceramics arises due to the effect of both grains as well as grain boundaries. The intersection of the smaller semicircle and larger semicircle with the Z' -axis gives the grain resistance R_g and grain boundary resistance R_{gb} of the material. The capacitance C_g and C_{gb} of each respective semicircle can be calculated

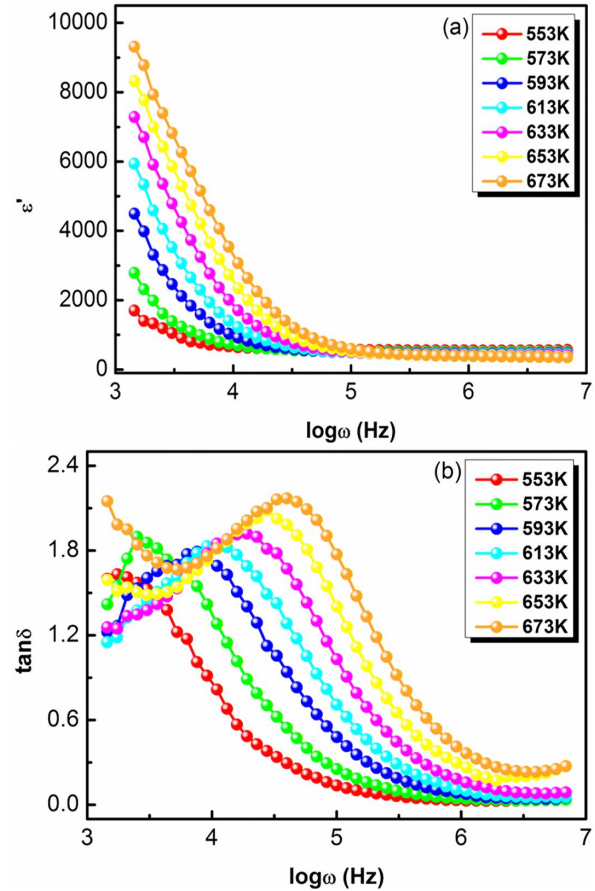


Fig. 3. Variation of (a) dielectric constant (ϵ') and (b) loss tangent ($\tan\delta$) with angular frequency at various temperatures for BZT ceramic.

by using the relation:

$$C = (R^{1-n}Q)^{1/n} \quad (1)$$

where n is the empirical exponent varying from 0 to 1; $n = 1$ stands for an ideal capacitor whereas n value becomes 0 for the ideal resistor. The obtained values of fitted parameters are listed in Table 2. The values of R_g and R_{gb} are found to decrease with increasing temperature, indicating a typical semiconductor behavior of the sample at high temperature. The high value of R_{gb} as compared to the R_g at all temperatures, is due to the lower concentration of oxygen vacancies and other charge carriers (e.g. trapped electrons and holes) in the grain boundaries. The values of activation energy E_a are calculated using Arrhenius plot of resistance data for R_g and R_{gb} as shown in Fig. 4b. A very small

difference in activation energy of grain and grain boundary suggests significantly low value of barrier height among the grain and grain boundary. A small barrier height indicates high densification of synthesized BZT ceramics.

The relaxation times τ for grain and grain boundary are calculated by using the relation of $\tau = RC$, where R is the resistance and C is capacitance value. The calculated τ values have been plotted versus inverse of absolute temperature T for both grain and grain boundary (Fig. 4c). The result shows that the relaxation time decreases with an increase in temperature, which suggests the presence of temperature dependent relaxation processes in the BZT compound. The activation energy estimated from the slope of the curve by using the equation:

$$\tau = \tau_0 e^{-E_a/k_B T} \quad (2)$$

where τ_0 is pre-exponential factor, E_a is activation energy, k_B is Boltzmann constant and T is the absolute temperature) is found to be 0.42 eV and 0.48 eV for grain and grain boundary, respectively.

We have also performed modulus spectroscopy to understand the relaxation mechanism in BZT. It is an important analytical tool because it can differentiate electrode polarization from grain boundary conduction processes, which is involved in the electrical relaxation of the material. It is also useful for separating components with similar resistance, but with different capacitances. The complex modulus is calculated by the following relations:

$$M^* = 1/\varepsilon^*(\omega) = M' + jM'' \quad (3)$$

$$M' = \omega C_0 Z'' \text{ and } M'' = \omega C_0 Z' \quad (4)$$

where ω is the angular frequency ($\omega = 2\pi f$) and C_0 is the geometrical capacitance. Fig. 5a and Fig. 5b show the variation of the real part of complex modulus M' and imaginary part of complex modulus M'' with angular frequency at different temperatures ranging from 553 K to 673 K. In Fig. 5a, M' has lower magnitude at lower frequency region and it shows continuous dispersion with increasing frequency. Fig. 5b shows an increase in

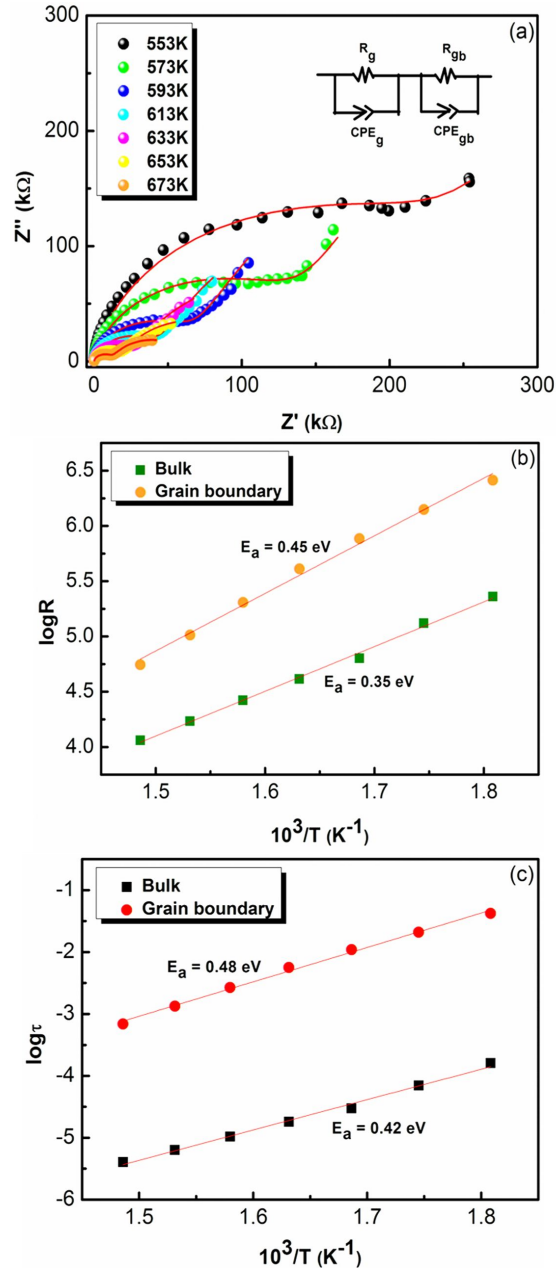


Fig. 4. (a) Nyquist plot of BZT ceramics with an equivalent circuit, (b) Arrhenius plot of grain and grain boundary resistance for BZT ceramics, (c) variation of relaxation time τ as a function of inverse of temperature.

the peak height of M'' with increasing temperature. The shift of maxima peaks M''_{\max} toward the high frequency side is observed with the rise in temperature. The sigmoidal increase in the value of M' is observed with increasing frequency for all

Table 2. Fitted parameters for grain and grain boundaries of BZT ceramics at different temperatures.

Temperature [K]	Grain				Grain boundary			
	R_g [k Ω]	Q_g [pF]	n	C_g [pF]	R_{gb} [k Ω]	Q_{gb} [pF]	n	C_{gb} [pF]
553	229	1470	0.914	697	2590	28500	0.80	15134
573	132	1310	0.904	525	1410	31000	0.809	14840
593	63	1290	0.903	468	768	36500	0.791	14224
613	41	1230	0.905	439	409	39200	0.798	13791
633	26	1230	0.901	394	203	45800	0.789	13148
653	17	1190	0.902	368	103	59300	0.770	12948
673	11	1130	0.906	352	56	78800	0.746	12375

the given temperatures, which is due to the short range mobility of charge carriers under the action of induced electric field. The increment of the peak height in M'' vs. $\log\omega$ plot is the result of reduction in the capacitance with increasing temperature and an important characteristics of a ferroelectric material above the ferroelectric-paraelectric phase transition temperature T_c . The frequency region below the relaxation peak in the imaginary part of the electric modulus M'' defines the region where carrier can move over long distances. Whereas, at frequencies above the peak, the motion of the charge carriers is confined and considered as mobile over short distances. The nature of modulus spectrum suggests that because of the difference in the charge carriers, there exists a hopping mechanism which contributes significantly to the electrical conductivity at an elevated temperature.

Fig. 6 illustrates the scaling behavior of “modulus master curve” for different temperatures. All the curves coincide into a single curve and almost perfectly overlap at different temperatures indicating that the dynamic process occurring in the sample at different frequencies exhibits the same temperature independent activation energy.

Fig. 7 shows the variation of electrical AC conductivity σ with angular frequency in BZT ceramics at different temperatures ranging from 553 K to 673 K. At low frequency region, conductivity shows frequency independent nature which is referred to as DC part of conductivity. The frequency independent DC conductivity has been explained by Funke [21] in the jump relaxation

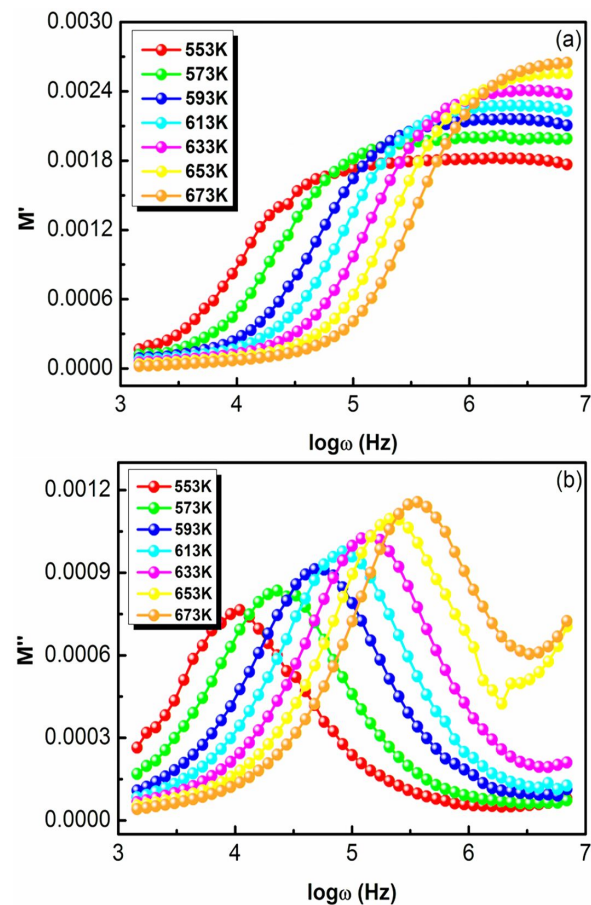


Fig. 5. Variation of (a) real and (b) imaginary part of modulus with angular frequency in BZT ceramics.

model (JRM). The frequency at which frequency independent phenomena switch to dependent ones is known as hopping frequency. The low frequency

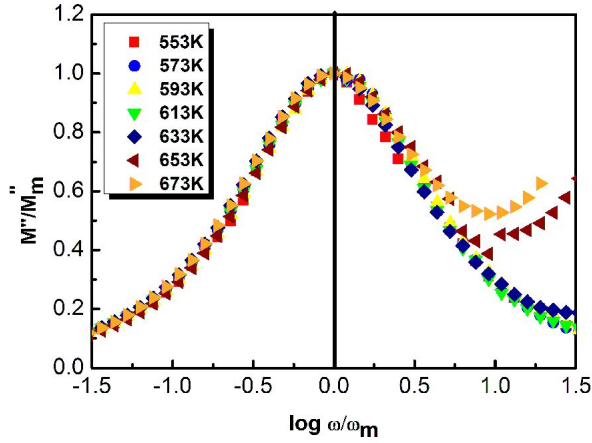


Fig. 6. Scaling behavior of M'' for BZT ceramics at different temperatures.

plateau region is shifted to the higher frequencies in the conductivity spectra with the increase in temperature. The high frequency conductivity shows dispersion which is possibly due to the tremendous increment of the mobility of the charge carriers. The total conductivity at a given temperature can be expressed by the double power law proposed by Jonscher [22]:

$$\sigma(\omega) = \sigma(0) + A\omega^{n_1} + B\omega^{n_2} \quad (5)$$

where $\sigma(0)$ is the DC part of conductivity which is frequency independent, A and B are pre-exponential factors and n_1 and n_2 are frequency exponents [23, 24]. It has been suggested that power law dispersion in electrical response of a material can be interpreted as a network of resistors R and capacitors C [25]. The network acts differently depending upon the AC conductivity in various frequency domains as:

1. At low frequencies, where $R^{-1} > \omega C$, current flows through the percolation paths of resistor across the network and the conductivity is therefore found to be frequency independent.
2. At intermediate frequencies, where $R^{-1} \sim \omega C$, current flows via both the components R and C contributing to the overall conductivity.

3. At high frequencies, where $R^{-1} < \omega C$, current flows through the network capacitance and AC conductivity rises.

It is noted that power law dependencies must occur in the frequency range, where the admittance magnitude of the capacitor ωC becomes comparable to the resistors R^{-1} .

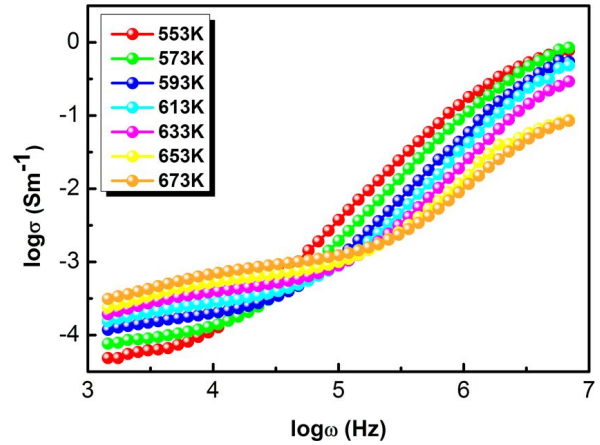


Fig. 7. Frequency dependent AC conductivity for different temperatures.

The temperature dependent variation of fitted parameter of exponents n_1 and n_2 are shown in Fig. 8. The exponent n_1 characterizing the low-frequency region, represents the non-diffusing modes and the exponent n_2 characterizing the high-frequency region, represents the existence of well-localized diffusing modes, respectively. Ishii et al. [26] predicted that in the lower frequency region, the exponent n_1 varies from 1 to 2 with an increase in temperature, while n_2 remains less than 1 at higher frequencies. From the plot, it is found that the value of both n_1 and n_2 decreases with the rise of temperature in contrast with quantum mechanical tunneling (QMT) model, which predicts that the exponent n is temperature independent [27]. According to the large overlapping polaron (LPT) model, n decreases with increasing temperature up to a certain temperature, then starts to increase with further rise in temperature [28], while in the small polaron tunneling (SPT) model, n increases with an increase of temperature [29]. Hence, the above mentioned LPT and SPT models are also not

applicable for the present sample studied. As the nature of the plot shows decreasing trend of the exponents n_1 and n_2 with an increase of temperature, the correlated barrier hopping (CBH) model is an appropriate model to describe the phenomena [30]. Hence, it can be concluded that according to the CBH model, classical hopping of charge carriers between localized sites over potential barrier is the most probable conduction mechanism for the BaZr_{0.1}Ti_{0.9}O₃ ceramics.

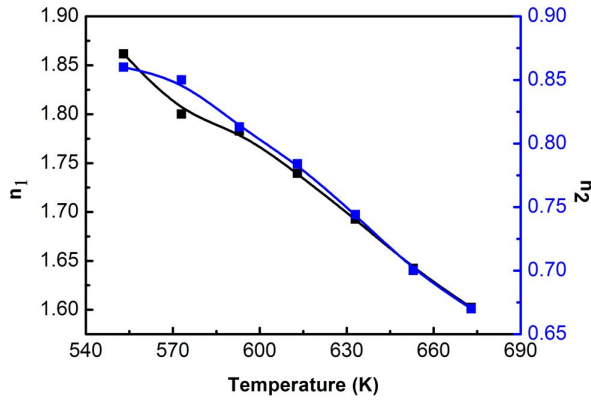


Fig. 8. Temperature dependent low and high frequency region exponents n_1 and n_2 of BZT ceramics.

According to CBH model, the minimum hopping distance R_{\min} is calculated by using the relation [31]:

$$R_{\min} = \frac{2e^2}{\pi\epsilon_0\epsilon W_m} \quad (6)$$

where e is the electronic charge, ϵ_0 is the permittivity of free space, ϵ is the dielectric constant of the material, and W_m is the binding energy, defined as the energy required to shifting a charge carrier completely from one to another site. The binding energy W_m can be estimated by using the following equation:

$$W_m = 6k_B T / (i - n) \quad (7)$$

where $i = 1$ or 2 corresponds to high and low frequency region.

Fig. 9 shows the variation of R_{\min} as a function of temperature at 1 kHz. It is observed that the value of R_{\min} decreases with temperature.

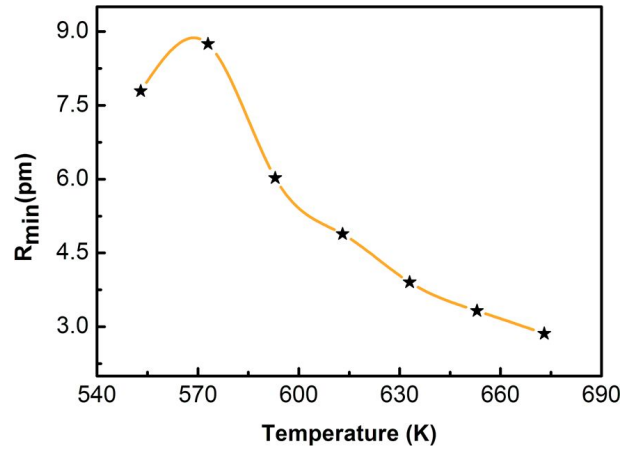


Fig. 9. Variation of minimum binding energy hopping distance R_{\min} with temperature at 1 kHz.

Further, if AC conductivity occurs from CBH model, then the density of states at Fermi level $N(E_f)$ is estimated by using the relation given below [32]:

$$\sigma_{ac}(\omega) = \frac{\pi}{3} e^2 \omega k_B T [N(E_f)]^2 \alpha^{-5} \left[\ln \frac{f_0}{\omega} \right]^4 \quad (8)$$

where e is the electronic charge, f_0 is the photon frequency and α is the localized wave function. The value of $N(E_f)$ is calculated by using equation 8 by assuming $f_0 = 10^{13}$ Hz and $\alpha = 10^{10} \text{ m}^{-1}$ at various operating frequencies and temperatures. Frequency dependent variation of $N(E_f)$ at different temperatures is shown in Fig. 10. It is seen that for a given temperature, the value of $N(E_f)$ initially decreases to a minimum and thereafter tends to a maximum with the increasing frequency. Further, it shows transition, i.e. the value of $N(E_f)$ increases systematically with the gradual increase in temperature from 553 K to 673 K in the low frequency region and then begins to decrease at high frequency region which is in a good consistency with the result of dielectric constant and AC conductivity studies. Therefore, at low frequency region, the electrical conductivity of the system is affected by both frequency as well as temperature, whereas at higher frequencies, charge carriers are transported to the localized sites by thermal agitation. The reasonably high values of $N(E_f)$ ($\sim 10^{19} \text{ eV}^{-1} \cdot \text{m}^{-3}$)

suggest that the hopping between the pairs of sites dominates the mechanism of charge transport in the present compound.

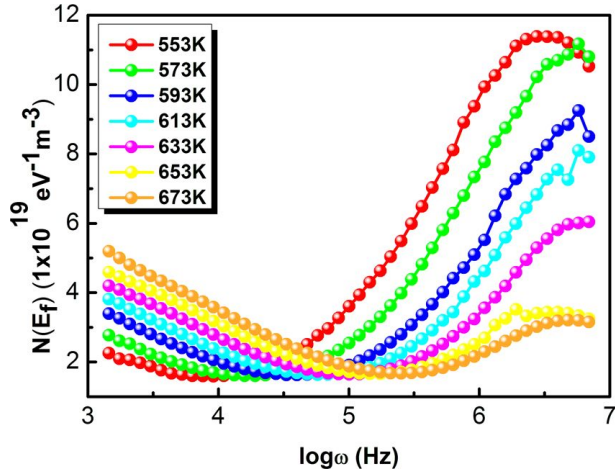


Fig. 10. Frequency dependent variation of density of states $N(E_f)$ at Fermi level at different temperatures.

Fig. 11 shows the variation of DC conductivity σ_{dc} versus inverse of absolute temperature ($10^3/T$). The activation energy E_a of the sample is calculated by using Arrhenius equation:

$$\sigma_{dc} = \sigma_0 e^{-E_a/k_B T} \quad (9)$$

where σ_0 is the natural conductivity, k_B is the Boltzmann constant and E_a is the activation energy of mobile charge carriers, respectively. The value of activation energy is found to be 0.32 eV in the mentioned temperature range. The calculated activation energy for the grain resistance (0.35 eV) and DC conductivity (0.32 eV) are very close in values which suggests a hopping mechanism for $\text{BaZr}_{0.1}\text{Ti}_{0.9}\text{O}_3$ ceramics.

The electronic thermal conductivity representing the total thermal conductivity can be determined using following equation [33]:

$$k = L\sigma T \left[1 + \left(\frac{3}{4\pi^2} \right) \left\{ \left(\frac{E_a}{k_B T} \right) + 4 \right\}^2 \right] \quad (10)$$

where L is the Lorentz number and T is the absolute temperature. Fig. 12 shows the thermal conductivity of grain as well as grain boundary for all

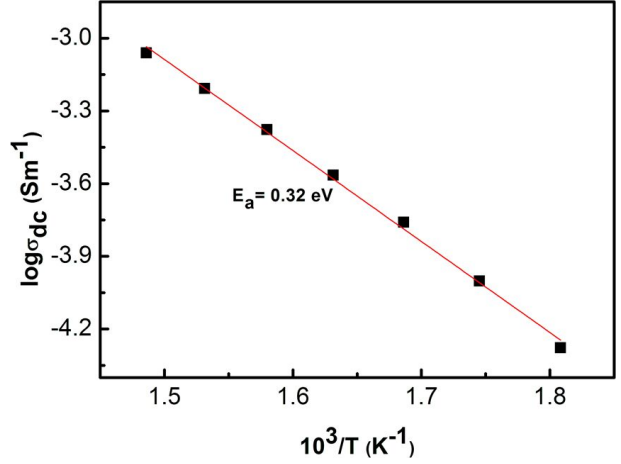


Fig. 11. Variation of DC conductivity σ_{dc} as a function of the inverse of absolute temperature $10^3/T$.

the temperatures. It can be observed that thermal conductivity for both the grain and grain boundary increases with the rise of temperature and exhibits very low values.

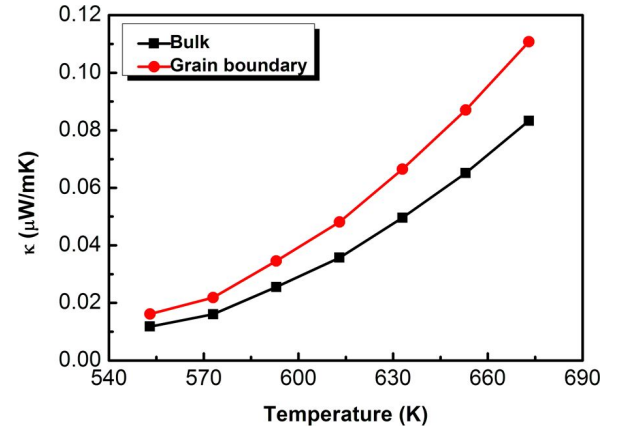
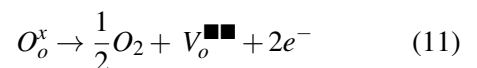


Fig. 12. Variation of electronic thermal conductivity for grain and grain boundary for BZT ceramics at different temperatures.

Generally, in perovskite titanates, ionization of oxygen vacancies creates conduction electrons by the reduction of Ti^{4+} to Ti^{3+} with the introduction of extra electron, and as given by Kröger-Ving equation [34]:



Therefore, the hopping of these electron or oxygen vacancies in the localized sites gives rise to the conduction process in the material. The oxygen vacancies can be generated in three different charge states, neutral V_o^x state, singly ionized V_o^\bullet state and double ionized $V_o^{\bullet\bullet}$ state. Activation energies between 0.1 eV to 0.5 eV and 0.6 eV to 1.2 eV are attributed to single ionized oxygen vacancies and double ionized oxygen vacancies, respectively, in perovskite oxides and for the AC conduction [35, 36]. Therefore, it can be concluded from the obtained value of activation energy that the singly ionized oxygen vacancies have a significant contribution to the conduction process of BZT.

4. Conclusions

In summary, dielectric relaxation and electrical conductivity of BaZr_{0.1}Ti_{0.9}O₃ ceramics have been investigated as a function of temperature and frequency. Further, to find a relation between electrical response characteristics of the material and the microstructural network, the complex impedance and AC conductivity of the material have been discussed in terms of an equivalent RC circuit. The overlapping of all peaks for different temperatures into a single peak in the modulus master curve confirms that the relaxation process exhibits the same mechanism at various temperatures with the same activation energy. The frequency dependent AC conductivity at different temperatures is found to obey the universal power law. The pair approximation type CBH model is found to be the appropriate model representing the universal behavior of the exponent n . The activation energy and the values of different parameters, such as R_{min} , $N(E_f)$ and k , have been estimated from AC conductivity. The obtained value of activation energy from DC conductivity indicates that the singly ionized oxygen vacancies are involved in the conduction process of BZT ceramics.

Acknowledgements

Tanusree Mondal acknowledges the Indian Institute of Technology (Indian School of Mines), Dhanbad, India, for providing the Senior Research Fellowship. Sayantani Das acknowledges to the University Grants Commission (UGC),

India, for providing the financial support in the form of Research Fellowship in Science for Meritorious Students (RFSMS).

References

- [1] LEE W.H., SU C.Y., *J. Am. Ceram. Soc.*, 90 (2007), 3345.
- [2] OHARA Y., KOUMOTO K., YANAGIDA H., *J. Am. Ceram. Soc.*, 68 (1985), 108.
- [3] PARK J.H., KAWAKAMI Y., SUZUKI M., AKEDO J., *Jpn. J. Appl. Phys.*, 50 (2011), 09ND19.
- [4] TANG P., TOWNER D.J., MEIER A.L., WESSELS B.W., *Appl. Phys. Lett.*, 85 (2004), 4615.
- [5] FARHI R., MARSSI M., SIMON A., RAVEZ J., *Eur. Phys. J. B.*, 9 (1999), 599.
- [6] DELUCA M., VASILESCU C.A., IANCULESCU A.C., BERGER D.C., CIOMAGA C.E., CURECHERIU L.P., STOLERIU L., GAJOVIC A., MITOSERIU L., GALASSI C., *J. Eur. Ceram. Soc.*, 32 (2012), 3551.
- [7] TANG X.G., CHEW K.H., CHAN H.L.W., *Acta Mater.*, 52 (2004), 5177.
- [8] MOURA F., SIMÕES A.Z., AGUIAR E.C., NOGUEIRA I.C., ZAGHETE M.A., VARELA J.A., LONGO E., *J. Alloy. Compd.*, 479 (2009), 280.
- [9] BHASKAR R.S., PRASAD R.K., RAMACHANDRA R.M.S., *J. Alloy. Compd.*, 509 (2011), 1266.
- [10] BHASKAR R.S., PRASAD R.K., RAMACHANDRA R.M.S., *J. Alloy. Compd.*, 481 (2009), 692.
- [11] SATEESH P., OMPRAKASH J., KUMAR G.S., PRASAD G., *J. Adv. Dielectr.*, 5 (2015), 1550002.
- [12] NATH K.A., PRASAD K., *Adv. Mater. Res.*, 2 (2012), 115.
- [13] KANG B.S., CHOI S.K., PARK C.H., *J. Appl. Phys.*, 94 (2003), 1904.
- [14] ANG C., YU Z., CROSS L.E., *Phys. Rev. B.*, 62 (2000), 228.
- [15] RODRIGUEZ-CARVAJAL J., *An introduction to the program FullProf 2000*, Laboratoire Léon Brillouin (CEA-CNRS) CEA/Saclay, France, 2001.
- [16] FERRARI M., LUTTEROTTI L., *J. Appl. Phys.*, 76 (1994), 7246.
- [17] HSIAO Y.J., CHANG Y.H., FANG T.H., CHANG Y.S., *Appl. Phys. Lett.*, 87 (2005), 142906.
- [18] JAWAHAR K., CHOUDHARY R.N.P., *Solid State Commun.*, 142 (2007), 449.
- [19] PRASAD A., BASU A., *Mater. Lett.*, 66 (2012), 1.
- [20] DUTTA A., BHARTI C., SINHA T.P., *Mater. Res. Bull.*, 43 (2008), 1246.
- [21] FUNKE K., *Prog. Solid State Chem.*, 22 (1993), 111.
- [22] JONSCHER A.K., *Nature*, 267 (1977), 673.
- [23] CHEN W., ZHU W., TAN O.K., CHEN X.F., *J. Appl. Phys.*, 108 (2010), 034101.
- [24] PELAIZ-BARRANCO A., GUTIERREZ-AMADOR M.P., HUANOSTA A., VALENZUELA R., *Appl. Phys. Lett.*, 73 (1998), 2039.
- [25] ALMOND D.P., BOWEN C.R., *Phys. Rev. Lett.*, 92 (2004), 157601.

- [26] ISHII T., ABE T., SHIRAI H., *Solid State Commun.*, 127 (2003), 737.
- [27] ELLIOTT S.R., *Adv. Phys.*, 36 (1987), 135.
- [28] YOUSSEF A.A.A., *Z. Naturforsch.*, 57a (2002), 263.
- [29] LONG A.R., *Adv. Phys.*, 31 (1982), 553.
- [30] IMRAN Z., RAFIQ M.A., AHMAD M., RASOOL K., BATOOL S.S., HASAN M.M., *AIP Adv.*, 3 (2013), 032146.
- [31] PRASAD K., BHAGAT S., AMARNATH K., CHOUDHARY S.N., YADAV K.L., *Mater. Sci.-Poland*, 28 (2010), 317.
- [32] SUBOHI O., KUMAR G.S., MALIK M.M., KURCHANIA R., *J. Mater. Sci.-Mater. Electron.*, 26 (2015), 9342.
- [33] JONSCHER A.K., *J. Mater. Sci.*, 16 (1981), 2037.
- [34] VERDIER C., MORRISON F.D., LUPASCU D.C., SCOTT J.F., *J. Appl. Phys.*, 97 (2005), 024107.
- [35] SMYTH D.M., *J. Electroceram.*, 11 (2003), 89.
- [36] MOOS R., HÄRDTL K.H., *J. Appl. Phys.*, 80 (1996), 393.

Received 2017-06-28

Accepted 2018-01-29